

Implications of Magma Transfer Between Multiple Reservoirs on Eruption Cycling

Derek Elsworth,^{1*} Glen Mattioli,² Joshua Taron,¹ Barry Voight,¹ Richard Herd³

Volcanic eruptions are episodic despite being supplied by melt at a nearly constant rate. We used histories of magma efflux and surface deformation to geodetically image magma transfer within the deep crustal plumbing of the Soufrière Hills volcano on Montserrat, West Indies. For three cycles of effusion followed by discrete pauses, supply of the system from the deep crust and mantle was continuous. During periods of reinitiated high surface efflux, magma rose quickly and synchronously from a deflating mid-crustal reservoir (at about 12 kilometers) augmented from depth. During repose, the lower reservoir refilled from the deep supply, with only minor discharge transiting the upper chamber to surface. These observations are consistent with a model involving the continuous supply of magma from the deep crust and mantle into a voluminous and compliant mid-crustal reservoir, episodically valved below a shallow reservoir (at about 6 kilometers).

Continuous and highly resolved geodetic and efflux records are available for only a few volcanoes. One of those is the Soufrière Hills volcano (SHV) on Montserrat, West Indies (1–3), which has been erupting since 1995. These data provide a window into deep processes contributing to stratovolcano behavior. We constrained magma migration with

wide-aperture geodetic data supplemented by a well-documented extrusion record, and used these to explore the effect of deeply sourced fluxes on short-term eruption periodicity. The global positioning system (GPS) array is capable of capturing magmatic exchange to a depth comparable to the distance across geodetic stations (~11 km).

The SHV has followed a pattern of seismic crises separated by about 30 years (4). The most

recent volcanoseismic crises, in the 1890s, 1930s, and 1960s, are interpreted as aborted eruptions, and the seismic crisis in the 1990s developed into the ongoing eruption. Phreatic activity began in July 1995 after several years of seismic unrest. The most recent eruption comprises a series of 2- to 3-year eruptive episodes and interspersed pauses lasting 1.5 to 2 years (1). An andesite dome grew continuously, in episode 1 from November 1995 until ~10 March 1998, followed by a pause with passive dome collapse ending in November 1999 (5). This cycle of growth of an active lava dome followed by a pause was repeated between December 1999 and mid-July 2003, followed by a pause lasting until October 2005 (6). Episode 3 began in October 2005 and ended in March 2007. A pause followed, which appears to have ended in August 2008 with continuing slow extrusion of lava on the western flank of the dome.

The inversion of ~1995–1997 GPS data suggests that the early magmas reside in a chamber at a depth of about 5 km (2, 7–9). Crystal phases in erupted magmas also imply that they

¹College of Earth and Mineral Sciences, Penn State University, University Park, PA 16802, USA; and Institute of Advanced Studies, University of Western Australia, Perth, Australia. ²Department of Geosciences, University of Arkansas, Fayetteville, AR 72701, USA. ³School of Environmental Sciences, University of East Anglia, Norwich NR4 7TJ, UK.

*To whom correspondence should be addressed. E-mail: elsworth@psu.edu

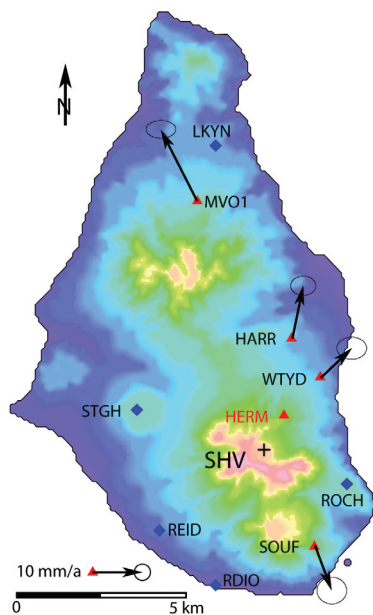


Fig. 1. Map of Montserrat, showing the location of the eruptive vent (black cross labeled SHV), continuous GPS sites (red triangles), and campaign GPS sites (blue diamonds) used in the flux analysis, and the Caribbean-fixed GPS velocity vectors for the period from 13 July 2003 through 1 November 2005, along with their 1σ errors for the continuous GPS (cGPS) sites. There is a strong radial deformation pattern relative to the vent, corresponding to inflation during this residual period (no surface magma flux). The proximal reference cGPS site HERM is shown in red.

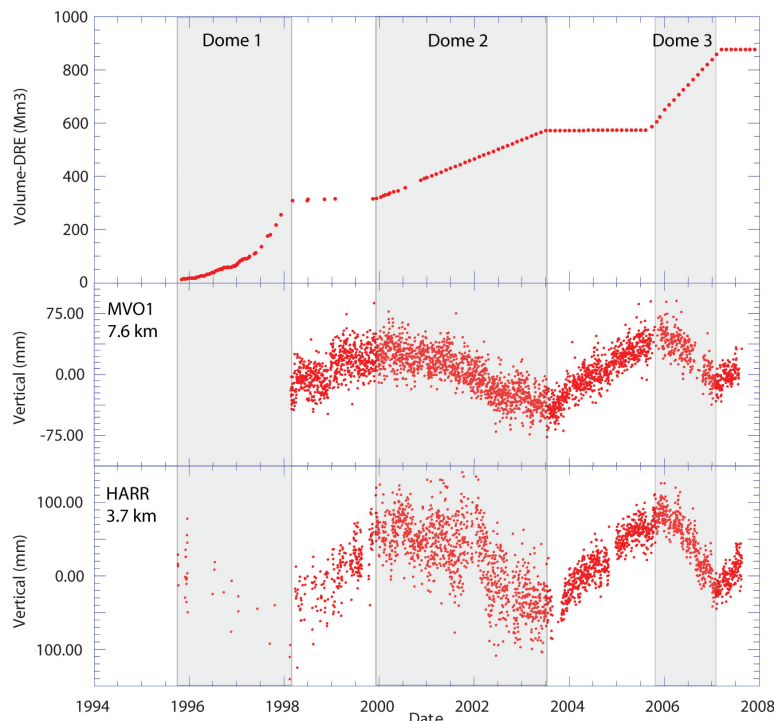


Fig. 2. Efflux of dense rock equivalent (DRE) from the SHV over time. Eruptive activity indicates three distinct active/repose cycles. Also shown is the evolution of station velocities within these prescribed cycles of activity. Resulting mean velocities are reported in table S1. Flux data from 1995 through early 1998 are from Sparks *et al.* (15) and data from 1998 are from electronically published MVO reports (6).

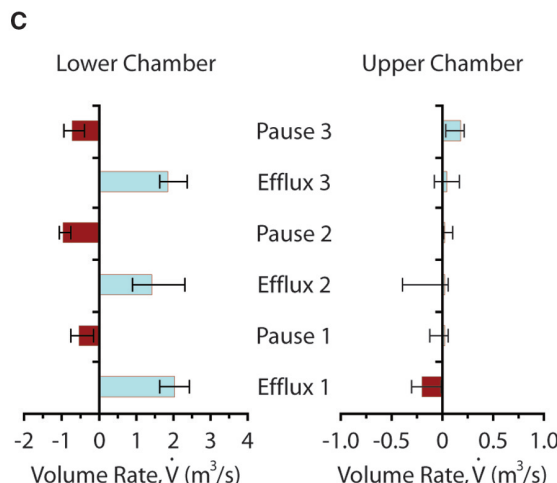
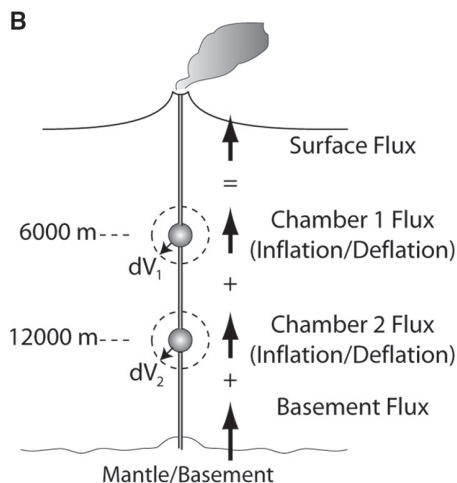
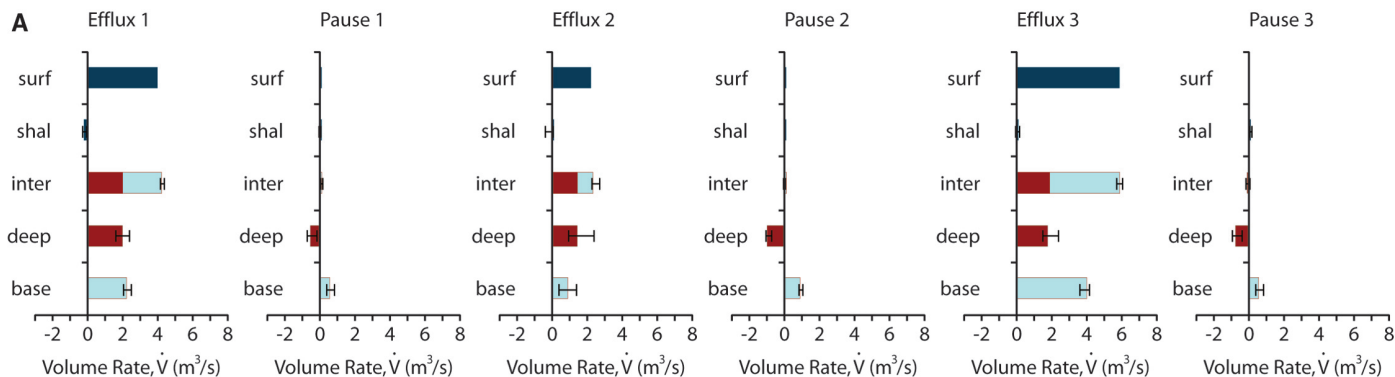
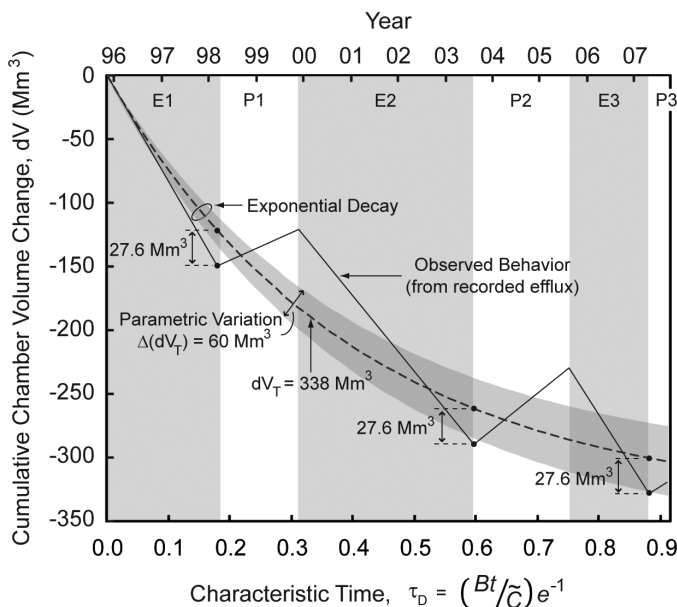


Fig. 3. (A) Average interchamber, basement supply, and chamber inflation rates recovered from co-inversion of surface efflux and geodetic data for dual-chamber geometry (B). Flux rates are in cubic meters per second of DRE, with surface efflux measured and all others calculated. Error bars denote the spread obtained from using data from the longest-aperture station (MVO1) together with data from stations SOUF, HARR, and WYTD. Chamber volume change rates (red, lower chamber; dark blue, upper chamber) are positive for deflation. Surface (surf, dark blue), interchamber (inter, red/blue), and basement (base, light blue) fluxes are each positive for upward flow. Shal, shallow. Interchamber flux is equivalent to the

sum of lower chamber deflation and basement supply (which passes through the lower chamber). Surface efflux is the sum of upper chamber deflation and interchamber transfer (pass-through). (C) Inflation (negative, red) and deflation (positive, blue) rates for each of the upper and lower chambers throughout the three sequences of eruption, with a pause after each one.

Fig. 4. Cumulative volume changes for the lower reservoir evaluated from the combined geodetic and efflux histories. E, eruption; P, pause. Modeled depletion is for a spherical chamber within an infinite elastic medium discharging through a vertical conduit. Parameters are as defined in table S2 (chamber radius, 1 km; depth, 12 km; conduit diameter, 30 m; shear modulus of rock, 3 GPa; bulk modulus of magma, 1.1 GPa; magma viscosity 55×10^6 Pa·s). $(Bt/\bar{C})e^{-1}$ represents the characteristic time for chamber depletion controlled by magma and chamber compressibility (\bar{C}) and efflux resistance (B).



were stable at pressures of ~ 130 MPa. The presence of small amounts of basalt mixed in the erupted andesite, however, implies that there is a

deeper supply of hot mafic magma (10, 11); some crystal phases also suggest that the upper chamber is connected to a deep reservoir at

depths of >10 km (12), and post-1997 geodetic data also support a source possibly as deep as 12 km (3). The substantial cumulative volume of the eruption (~ 0.9 km³) and its decade-long continuity and chemical consistency, coupled with observations of co-eruptive displacements, suggest that the upper magma source is voluminous: ~ 4 km³ (13). Together, these observations constrain a model of two stacked magma reservoirs, at depths of ~ 6 and ~ 12 km, connected from the surface to the deep crust and mantle by vertical conduits. Although some evidence suggests that the shallow conduits may be planar (2, 14), the observed surface deformation was radial around the volcano throughout most of the 1997–2007 period (Fig. 1). Correspondingly, the volumetric response of the reservoirs to inflation and deflation appears to dominate the far-field geodetic response, and only these are considered here.

For this model of two stacked magma reservoirs (fig. S1), we co-invert surface efflux and GPS station velocities to recover rates of crustal magma transfer throughout the 12-year duration of the eruption. The three eruptive episodes had sustained surface fluxes of 2 to 8 m³/s, punctuated by periods of repose with flux $\ll 1$ m³/s (Fig. 2 and Fig. 3A). Over this period, radial

and vertical ground surface velocities are continuously available for at least four GPS stations (Fig. 2). Stations typically show net outward- and upward-deformation during repose and inward- and downward-deformation during renewed surface efflux. Displacement histories are converted to mean surface velocities within each effusive episode or pause (table S1). Mean surface velocities for each of two independent stations (table S1) are then co-inverted with surface efflux [supporting online material (SOM)] to calculate magma migration rates through the intermediate and deep crust (SOM). The mean velocity of the most distal station (MVO1 at ~11 km) (Fig. 1) is combined sequentially with each of the three proximal stations to recover three independent measurements of inflation rates and fluxes, shown in Fig. 3 for each of three cycles of eruption followed by a pause (SOM). These results for an incompressible magma (Fig. 3) are representative of calculations for compressible magma for the chamber depths examined here (figs. S2 and S3).

For each of the three eruptive episodes, the co-inversion of the geodetic and efflux data shows that (Fig. 3) the surface efflux responds to volume and pressure changes at a deep level, rather than being a result simply of deflation of a shallow reservoir, as usually presumed. This is apparent in Fig. 3A as an increased magma supply from the basement into the lower chamber, coupled with an active deflation of the lower chamber. For our two-chamber model, the additive flux from these two deeper sources issues into, and causes outflow from, the shallower chamber and upper magmatic system with little volume loss, comprising almost the entire surface efflux in all three active episodes. The only apparent volumetric loss between the deep magmatic system and the surface is manifested as calculated minor inflations (episode 1) or deflations (episodes 2 and 3) of the upper reservoir. Although the upper reservoir is not actively involved as a dynamic storage element, the deeper-sourced material is unlikely to directly transit the upper chamber during a single eruptive episode. The volume change of a spherical reservoir (dV) is proportional to both the pressure change in the magma (dp) and chamber volume (V) and inversely proportional to rock shear modulus (G_R) as $dV \sim (V/G_R)dp$ (SOM eq. 3). For a shear modulus of 1 GPa (SOM), co-eruptive inflationary and deflationary volumes of the upper reservoir on the order of $10 \times 10^6 \text{ m}^3$ imply pressure changes of $<3 \text{ MPa}$ for chamber volumes $>4 \text{ km}^3$. For similar moduli and chamber volumes in the lower reservoir, co-eruptive volume changes are an order of magnitude larger ($\sim 150 \times 10^6 \text{ m}^3$) and imply co-eruptive pressure drops that are an order of magnitude greater. Correspondingly, the small deformational signal from the upper reservoir implies that either pressure changes are small and the upper system is largely open, or the upper reservoir is smaller and more geometrically rigid in

comparison to a more voluminous lower chamber. Independent geodetic and petrologic evidence identifying the substantial volume of the upper chamber ($>4 \text{ km}^3$) favor the presence of an open system.

For the most vigorous of the active phases (episodes 1 and 3, with fluxes for some periods exceeding $7 \text{ m}^3/\text{s}$; Fig. 3), the basement flux was larger than the contribution supplied by deflation of the lower reservoir. If the antecedent eruption was particularly vigorous, and therefore substantially depleted the lower reservoir, then this trend was reversed, and the relatively weaker episode 2 was primarily sustained by draining the lower chamber to force out shallower magma. Indeed, for the weak episode 2 (with surface flux steady at $2.2 \text{ m}^3/\text{s}$) (Fig. 3), the basal supply was indistinguishable from either the previous or subsequent periods of repose, both of which had fluxes of roughly $1 \text{ m}^3/\text{s}$.

During the eruptive pauses, the co-inverted data imply that supply of magma into the basal crust continued at $\sim 1 \text{ m}^3/\text{s}$, and the lower reservoir re-inflated. Although the lower system appears to have been recharging itself for the next eruptive episode, the upper and lower magmatic systems remained connected, and surface efflux continued at about the same rate of combined supply between the lower and upper reservoirs: Inter-reservoir transfer approximately mirrored the surface efflux (~ 0.1 to $1.0 \text{ m}^3/\text{s}$). Again, the absence of a significant inflationary or deflationary signal in a voluminous upper reservoir as the lower chamber either fills (inflates) or discharges (deflates) suggests that the upper system is open and cannot sustain substantial overpressures transmitted from below. Valving of the flow system between the upper and lower reservoirs is consistent with this observation that the lower reservoir can refill while the upper system remains open. This valving must prevent substantial influx of magma from the lower to the upper chamber during periods of pause, and its charge of either heat or gas, in driving the invigorated system.

With the change from pauses to eruptive phases, magma supply to the deep reservoir continued at a minimum rate of $\sim 1 \text{ m}^3/\text{s}$, augmented to rates of $\sim 5 \text{ m}^3/\text{s}$. The co-inverted data indicate that the eruptive episodes deplete the lower reservoir only, and not the upper reservoir, which may even inflate slightly as inflow slightly outpaces outflow. During subsequent periods of pause, the deep reservoir re-inflates, but typically at half the rate of its previous depletion. Because periods of repose were typically shorter than the periods of active depletion (eruption), the deep reservoir was being depleted (deflated) throughout this decade-long episode. The cumulative volume change for the deep reservoir is illustrated in Fig. 4, indicating that over 12 years, the lower chamber has deflated stepwise by $\sim 320 \times 10^6 \text{ m}^3$, while the upper reservoir inflated by $8 \times 10^6 \text{ m}^3$ (constituting an inflation of $14 \times 10^6 \text{ m}^3$ up to 1998, followed by de-

flation by $6 \times 10^6 \text{ m}^3$ over the remaining decade). This net deflation of the system of $\sim 320 \times 10^6 \text{ m}^3$ is about one-third of the total effusion of $\sim 0.9 \text{ km}^3$ recorded to date, requiring that the remainder of the magma ($\sim 570 \times 10^6 \text{ m}^3$) has been sourced from below the lower reservoir. These observations may be compared with models that represent the efflux history from a deflating spherical chamber in an elastic medium (SOM), as illustrated in Fig. 4. This matches the average deflationary history, as shown, and yields a predicted ultimate eruptive volume of $338 \times 10^6 \text{ m}^3$ from the lower chamber with $\sim 320 \times 10^6 \text{ m}^3$ ($\sim 95\%$) transferred to March 2007 (Fig. 4). Although the upper reservoir has been interpreted to be voluminous, on the order of a few cubic kilometers, it is apparent that the major changes in magma storage that have supplied the eruption are from depth ($>12 \text{ km}$), with the lower reservoir contributing only a third of the erupted volume.

References and Notes

1. T. H. Druitt, P. Kokelaar, Eds., *The Eruption of Soufriere Hills Volcano, from 1995 to 1999* (Memoir 21, Geological Society of London, London, 2002).
2. G. S. Mattioli *et al.*, *Geophys. Res. Lett.* **25**, 3417 (1998).
3. G. S. Mattioli, R. Herd, *Seismol. Res. Lett.* **74**, 230 (2003).
4. S. R. Young *et al.*, *Geophys. Res. Lett.* **25**, 3389 (1998).
5. G. Norton *et al.*, in (1), pp. 467–482.
6. Montserrat Volcano Observatory, reports from 1995 to 2008, available at www.mvo.ms.
7. W. P. Aspinall *et al.*, *Geophys. Res. Lett.* **25**, 3397 (1998).
8. J. Barclay *et al.*, *Geophys. Res. Lett.* **25**, 3437 (1998).
9. B. Voight *et al.*, *Science* **283**, 1138 (1999).
10. C. Annen, J. D. Blundy, R. S. J. Sparks, *J. Petrol.* **47**, 505 (2006).
11. M. D. Murphy, R. S. J. Sparks, J. Barclay, M. R. Carroll, T. S. Brewer, *J. Petrol.* **41**, 21 (2000).
12. J. D. Devine, M. J. Rutherford, G. E. Norton, S. R. Young, *J. Petrol.* **44**, 1375 (2003).
13. B. Voight *et al.*, *Geophys. Res. Lett.* **33**, L03312 (2006).
14. A. Costa, O. Melnik, R. S. J. Sparks, B. Voight, *Geophys. Res. Lett.* **34**, L02313 (2007).
15. R. S. J. Sparks *et al.*, *Geophys. Res. Lett.* **25**, 3421 (1998).
16. We thank M. Strutt, G. Ryan, and P. Williams of the Montserrat Volcano Observatory and W. Johnston for maintenance of the cGPS network on the SHV. This work is a result of partial support from NSF under awards NSF-CMS-9908590, NSF-CD-0607691, NSF-CD-0507334, and NSF-CD-0607782. The Caribbean Andesitic Lava Island Precision Seismo-geodetic Observatory (CALIPSO) Facility was supported by grants NSF-IF-0523097 and NSF-IF-0732728, and this support is gratefully acknowledged. The conclusions reported here are those of the authors.

Supporting Online Material

www.sciencemag.org/cgi/content/full/322/5899/246/DC1
Methods

Figs. S1 to S3

Tables S1 and S2

References

3 June 2008; accepted 10 September 2008
10.1126/science.1161297